acoustics

MDPI

Article

FEM-BEM Vibroacoustic Simulations of Motion Driven Cymbal-Drumstick Interactions

Evaggelos Kaselouris [1,2], Stella Paschalidou [3], Chrisoula Alexandraki [3] and Vasilis Dimitriou [1,2,*]

[1] Physical Acoustics and Optoacoustics Laboratory, Department of Music Technology & Acoustics, Hellenic Mediterranean University, 74133 Rethymnon, Greece
[2] Institute of Plasma Physics and Lasers, Hellenic Mediterranean University Research Centre, 74100 Rethymno, Greece
[3] Department of Music Technology & Acoustics, Hellenic Mediterranean University, 74133 Rethymnon, Greece
* Correspondence: dimvasi@hmu.gr

Abstract: The transient acoustic dynamics of a splash cymbal are investigated via the Finite Element Method-Boundary Element Method. Real three-dimensional motion data recorded from the interaction of drummer–drumstick–cymbal provide the initial and the loading conditions to the simulated interaction of the drumstick–cymbal Finite Element Models. Progressively intensified free strokes are used as loading conditions for both experiment and simulation. The velocity values of the moving drumstick in various drumming conditions are monitored, recorded, and analysed to provide input data into the time domain simulations. The synergy of motion capturing and numerical methods allows computing the sound generated by the combined interaction of the vibroacoustic behaviour of the cymbal with the motor-interaction of the performer. The proposed methodology promotes a novel perspective in musical instrument design, optimization, and manufacturing considering performance discrepancies intentionally introduced by performers.

Keywords: cymbal; drumstick; vibroacoustics; FEM-BEM modelling and simulation; motion capture

Citation: Kaselouris, E.; Paschalidou, S.; Alexandraki, C.; Dimitriou, V. FEM-BEM Vibroacoustic Simulations of Motion Driven Cymbal-Drumstick Interactions. *Acoustics* **2023**, *5*, 165–176. https://doi.org/10.3390/acoustics5010010

Academic Editor: Yat Sze Choy

Received: 9 January 2023
Revised: 30 January 2023
Accepted: 31 January 2023
Published: 2 February 2023

1. Introduction

Cymbals are common percussion instruments and irreplaceable parts of drum sets. The history of these idiophone musical instruments existed since ancient times, when they were played by being hit in various ways, most commonly, by a drumstick or by another cymbal. Drum cymbals are essential to all kinds of drum kits for any type of music. They are used in percussion ensembles, jazz bands, rock bands, and marching bands, as well as in large orchestras. Commonly, drum sets include at least four different types of cymbals, namely, splash, crash, ride, and hi-hat cymbals. The sound produced by a cymbal is complex and is intrinsically related to its vibrational characteristics, which depend on its dimensions, its shape, and its material [1,2]. Usually, cymbals are manufactured by copper-based alloys. Depending on the manufacturer and the type of cymbal, small amounts of other elements, such as aluminium, silver, gold, and phosphorus, may be aggregated to copper. Bronze alloys like B20 (80 percent copper, 20 percent tin) and B8 (92 percent copper, 8 percent tin) are nowadays commonly used by well-known cymbal manufacturers [3]. Furthermore, brass alloys of copper and zinc are chosen for the manufacturing of cymbals with predefined acoustic characteristics.

The vibrational characteristics of cymbals using experimental methods such as electronic speckle pattern interferometry and laser vibrometry have been studied in [4,5]. More than a hundred normal modes were identified using experimental measurements validated by Finite Element Method (FEM) simulations in [6,7]. The correlation between the percussive sound and the residual stress/strain distributions in a cymbal was studied in [8], while the effect of the manufacturing process of hammering on the vibrational behaviour of cymbals was evaluated in [9] via FEM simulations. Nonlinear vibrations of plates with

variable thickness and their application to synthesising cymbals sounds were investigated in [10,11]. Moreover, the inclusion of washers and sticks/mallets in the sound synthesis of cymbals was recently investigated in [12] via coupled finite difference and FEM models, while the relationship between chaotic vibrations and acoustic properties of percussion cymbals was studied by experimental measurements [13]. In [14], advanced numerical simulations that include modal and frequency response function finite element analysis, frequency domain, and time domain FEM-boundary element method (BEM) analysis were performed to study the vibroacoustic behaviour of crash and splash cymbals. The results of the modal analysis agree with the experimental measurements found in the relevant literature. However, to the authors' knowledge, the motion of the real drumstick for the excitation and vibration of cymbals has neither been studied, nor even considered in the articles referenced herein.

In this research work, we focus on introducing the real motion data of the moving drumstick interacting with a cymbal in the coupled vibroacoustic numerical simulations. A FEM-BEM time domain simulation describes the transient acoustodynamics of a B20 bronze alloy splash cymbal. The real 3D motion data recorded during the interaction of drummer–drumstick–cymbal define the displacement, velocity, and acceleration values of the moving drumstick in various drumming conditions, providing the actual loads to the numerical models. A qualitative comparison of recorded and simulated sound is also performed to reveal whether changes of the recorded sound are manifested in the sound produced by the simulation. Combining motion capturing with FEM-BEM multiphysics simulations allows the computation of the generated sounds during drumstick–cymbal interactions considering the performance discrepancies intentionally introduced by performers.

2. Mathematical Modelling

FEM and BEM are valuable mathematical methods that are able to simulate the vibroacoustic behaviour of musical instruments when they interact with any type of force loads, vibrations, and variations in environmental conditions (i.e., temperature, humidity) [15–17]. In this study, time domain FEM-BEM simulations are performed. The fundamental equation of motion for structural analysis in a matrix form is:

$$[M]\left\{\frac{\partial^2 U}{\partial t^2}\right\} + [C]\left\{\frac{\partial U}{\partial t}\right\} + [K]\{U\} = \{F\} \tag{1}$$

where $[M]$ is the mass matrix, $\{U\}$ is the displacement vector, $[C]$ is the damping matrix, $[K]$ is the stiffness matrix, and $\{F\}$ is the load vector. The damping in the system can be defined using a stiffness matrix multiplier that forms the viscous damping matrix as $[C] = \beta[K]$, where β is the Rayleigh damping constant.

The time domain FEM-BEM mathematical model is solved by the LS-DYNA [18], which can provide an integrated solution for vibroacoustic problems by coupling the FEM transient dynamic solver with the BEM acoustic solver. The air surrounding the vibrating structure is modelled by BEM, which computes the pressure of the radiated sound. For the time domain FEM-BEM analysis, initially the time domain FEM analysis is performed, and the time domain dynamic response of the structure is converted to the frequency domain via the Fast Fourier Transform (FFT). Then, the computed boundary velocities provide the boundary velocities for the subsequent BEM acoustic computations [17].

The Helmholtz equation governs the acoustic wave propagation of the BEM frequency domain analysis in an ideal fluid, with no presence of any volume source [19]:

$$\nabla^2 p + k^2 p = 0 \tag{2}$$

where p is the acoustic pressure and k is the wavenumber. By Green's theorem, Equation (2) is transformed to an integral equation. Thus, the pressure at any point in the fluid medium is expressed as an integral of surface pressure and surface velocity of a vibrating structure:

$$P_Q(\omega) = \int_S (G\frac{\partial p(\omega)}{\partial n} - p(\omega)\frac{\partial G}{\partial n})dS \tag{3}$$

where $P_Q(\omega)$ is the sound pressure at a field point Q, S is the structure surface, n is the normal vector on the surface S, $p(\omega)$ is the surface pressure, ω is the angular frequency of the acoustic wave, and G is the Green's function, given by:

$$G = \frac{e^{-ikr}}{4\pi r} \tag{4}$$

where r is the distance between the surface integration point and the field point Q. For vibroacoustic problems, the conservation of momentum at the boundary surface of the vibrating structure leads to the following boundary condition:

$$\partial p(\omega)/\partial n = -i\rho\omega v_n(\omega) \tag{5}$$

where ρ is the acoustic fluid density and $v_n(\omega)$ is the normal velocity on the surface S. This equation relates the normal derivative of pressure to the normal velocity. Thus, the knowledge of pressure and velocity on the surface is sufficient to determine the pressure at every field point.

3. Modelling and Simulation

The CAD geometry of an 8-inch (20.32 cm) splash Zildjian cymbal [20] is designed along with the geometry of a wooden drumstick [21], as shown in Figure 1. The diameter of the bell for the splash cymbal is 78 mm and its inner diameter is 12.3 mm. The thickness from the centre to the edge of the cymbal varies and at the edge becomes 0.5 mm. The length of the drumstick is 39.4 cm. The cymbal is modelled as a deformable body, while the drumstick is modelled as a non-deformable rigid body.

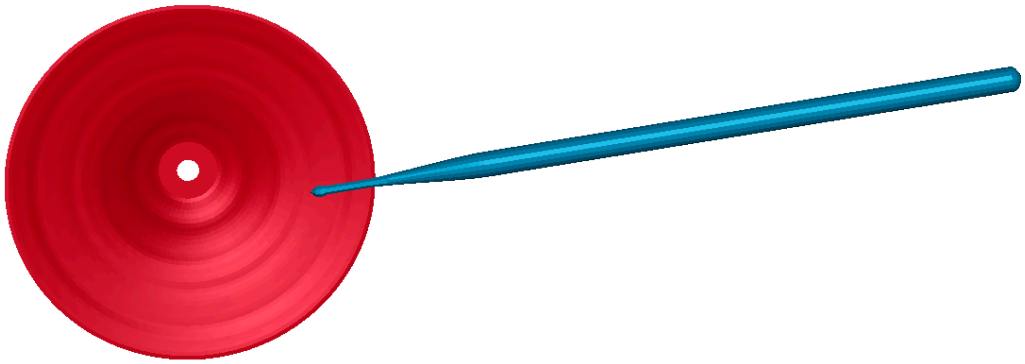

Figure 1. The CAD models of the splash cymbal and the drumstick.

The CAD geometry of the cymbal is discretized by approximately 20,000 shell elements, generated after a mesh independent study, by quadrilateral shell elements. The material properties of the B20 bronze alloy are set according to [22]. The density is 8607 kg/m^3, the Young's modulus is 112.6 GPa, and the Poisson's ratio is 0.342. The material properties for hickory wood, used for the drumstick, are also considered from the literature [23]. The precise values of the parameters describing the material of the cymbal and that of the drumstick are crucial for the simulation results. The Rayleigh damping constant is 0.001 [9]. Regarding the boundary conditions, displacements are fixed for the nodes bounding the central hole, simulating the real cymbal's support structure [6,14]. The mechanical vibrational timestep for the transient analysis is 1 µs.

A frequency range of 0–8000 Hz is considered for the time domain FEM-BEM vibroacoustic simulations. The output frequencies are also set to this range, while the resolution is set to 1 Hz. The air is the acoustic medium at the room temperature with a density of 1.21 kgm^{-3} and sound speed of 340 ms^{-1} at a reference pressure of 20 μPa. The geometry of the air sphere that surrounds the drumhead consists of 2000 BEM elements. A massless acoustic node is set 0.5 m above the impact point of the cymbal, which is considered to have coordinates (X,Y,Z) = (0,0,0) m, where X corresponds to the distance of length, Y corresponds to the distance of width, and Z corresponds to the distance of height. This node corresponds to an assumed microphone position in the acoustic field, where the sound pressure arising from the impact is measured. The spatial position of the drumstick with reference to the cymbal and its velocity values under different drumming conditions, captured by a 3D motion capture system, are imported as initial and loading conditions in the time domain FEM-BEM model, as described in detail in the following section. Moreover, it should be mentioned that, in [14], time domain FEM-BEM vibroacoustic simulations for the models of crash and splash musical cymbals were performed; however, the drumstick was not modelled and the real recorded experimental data for its motion were not considered.

The time dependent FEM-BEM simulations of the drumstick—cymbal interaction model have high computational needs and are runtime demanding simulations. Therefore, like in our previous works [14,15,24], the High-Performance Computer (HPC) ARIS for parallel processing [25] is used for the simulations. A typical runtime for a sampling rate of 16 kHz for the vibroacoustic analysis in the HPC system is 1600 core-hours.

4. Experimental Work

A marker-based motion capture (mocap) system is used for capturing the real loading conditions to be used in the FEM-BEM simulations. Specifically, 3D position data of sub-millimetre accuracy are recorded by a passive optical system (Optitrack V120:Trio) comprising a rig of six infrared high-speed wide-angle cameras (Optitrack Prime^x 13W) at a sampling rate of 120 Hz. A rigid body is created on the drumstick by three reflective markers (Figure 2); two positioned along its axis—just before and after the hand gripping position—and one by wrapping the drumstick head by an adhesive reflective material. A single (unlabelled) reflective marker is also placed on the very top of the cymbal stacker, 38 mm above the cymbal central point; this reference marker is used for detecting moments of contact between drumstick and cymbal as explained later in this section. Another rigid body of unique geometry is also used for recording wrist position, as has been previously done for full-body motion tracking in [26,27].

Monophonic audio is recorded by a LineAudio CM4 cardioid condenser microphone placed ca. 50 cm over the cymbal, half-way between centre and rim through a Sound Devices MixPre-10 II audio recorder at 96 kHz. Additionally, a cheap piezo contact microphone is attached to the base of the boom arm as an indicator of approximate moments of contact begin between the drumstick and the cymbal. All reflective objects and materials are covered to avoid reflections that could be falsely detected as markers. Six progressively intensified strokes (dynamic levels corresponding to pianissimo, piano, mezzo-piano, mezzo-forte, forte, and fortissimo, which, in music notation, are coded by the following symbols: *pp, p, mp, mf, f, ff*) are performed by a professional drummer, during which the drumstick is free to rebound; all strokes are at a specific position on the drumhead (2/3 off centre) and are at a fixed (maximum) mounting bolt tension. The experimental setup is video recorded by three high-speed cameras (GoPro 4 Black) positioned at different angles. All data (mocap, audio, video) are manually time-aligned at post-processing based on a clapboard, to which two reflective markers are attached. The experimental setup, along with a perspective view of the coordinate system attached to the centre of the Optitrack V120:Trio system, is illustrated in Figure 2. The characteristics and the material properties of the cymbal and drumstick for motion capturing were described in Section 3, and the central hole of the cymbal is structurally fixed, following the simulation's boundary conditions.

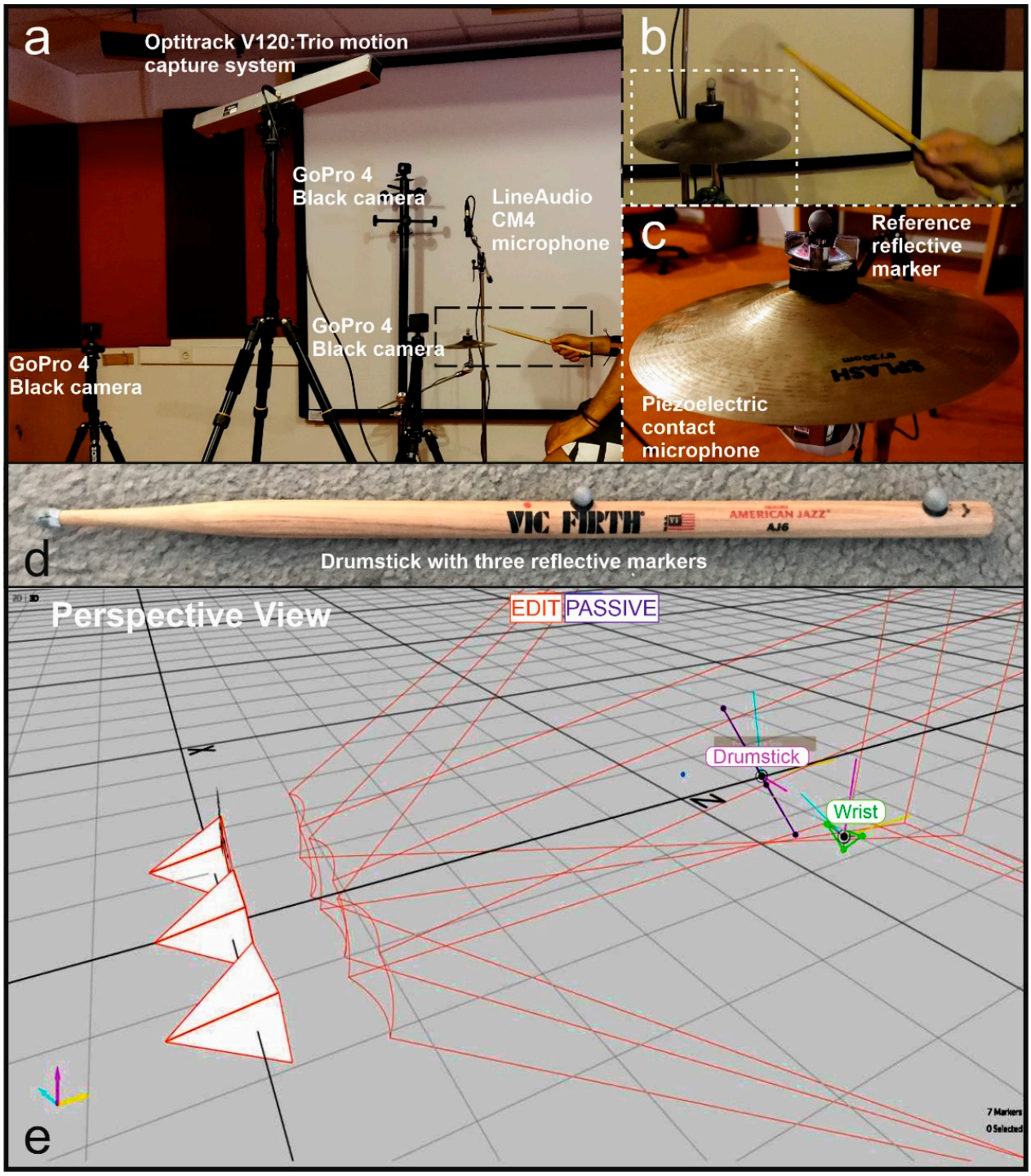

Figure 2. (**a**) Experimental setup demonstrating the Optitrack V120:Trio motion capture system, three reference cameras, the LineAudio CM4 microphone, the cymbal, and the drummer, (**b**) zoomed detail of (**a**) in the cymbal–drummer positioning, (**c**) zoomed detail of (**b**) in the cymbal, the reference marker, and the piezoelectric contact microphone, (**d**) drumstick with the three reflective markers attached, (**e**) coordinate system origin attached to Optitrack V120: Trio system.

The average collision force is equal to the rate of change of momentum or proportional to the rate of change of velocity (before and after collision):

$$\{F\} = \left\{\frac{\Delta p}{\Delta t}\right\} = [M]\left\{\frac{\Delta v}{\Delta t}\right\} = [M]\left\{\frac{v_{fin} - v_{init}}{\Delta t}\right\} \quad (6)$$

where $\Delta p/\Delta t$ is the rate of change of momentum, $\Delta p = [M]\Delta v$, Δv is the change of velocity, and $[M]$ is the mass matrix. For a hard collision, the maximum force is double its mean value, and, for simplicity reasons, is also considered to be the case for the splash cymbal set at maximum tension on the mounting bolt in the experiment.

The effective mass used in each individual drum stroke may vary depending on the grip technique (the fulcrum point used), as well as the overall arm gesture and its spatial trajectory [28]. Hence, it is hard to find a reliable way to calculate the implicated mass. Thus, mass is neglected by approaching it as a common factor for both simulated and real excitation, and the relative force is computed instead as being proportional to the rate of velocity change. Therefore, only the recorded velocity and the spatial coordinates of the drumstick and the cymbal are adopted by the FEM-BEM model. Other experimental approaches have been used in the past to directly capture force-related measures, such as by placing sensors for either force (piezoelectric crystals, [29]) or stress (strain gauges, [30]) onto the drumstick or the instrument itself. To secure the quality of the drumming gestures by the musician, as well as the vibrational and acoustic properties of the instrument, the experimental setup is free of sensors and cables that would be otherwise attached on the drumstick and the cymbal.

Position data from the motion capture system are expressed in meters in relation to a fixed coordinate system, with its origin attached to the centre of the V120:Trio system. The data are processed in Matlab. Missing data are filled by interpolating the last sample before, with the first sample after each gap; this process is only required at moments that did not coincide with the striking gestures. To address limitations imposed by the sampling rate of the mocap system, all data are treated through a linear interpolation. Velocity and acceleration values are computed by the *mctimeder* in the Mocap Toolbox (v1.5) as an estimation of the first-/second- order time derivative. To compress noise produced by the differentiation, a Savitzky–Golay FIR smoothing filter, with a seven-frame window length, of the following general form, is used [31]:

$$y[n] = \sum_{m=n-M}^{n+M} h[n-m]\, x[m] \tag{7}$$

where $y[n]$ is the output sequence at a central point n, $x[m]$ the observed values at the discrete samples m within the approximation interval, of which M is its half width, and $h[n-m]$ the shifted impulse responses for any group of $2M + 1$ input samples. This is a type of least-squares polynomial smoothing that uses $(2M + 1)$ neighbouring elements to fit to a polynomial of some order, with M being equal to or greater than the order of the polynomial. In Matlab, the *sgolayfilt* applies the smoothing filter to the data for a user-defined polynomial order and frame length.

Figure 3 (bottom) illustrates the z-position, velocity, and acceleration of the drumstick head for 200 frames around its lowest z-position for three representative free strokes, namely, *p*, *mf*, *ff*, while Figure 3 (top) displays the gesture traces of all reflective markers and centroids of rigid bodies for the last, hardest stroke.

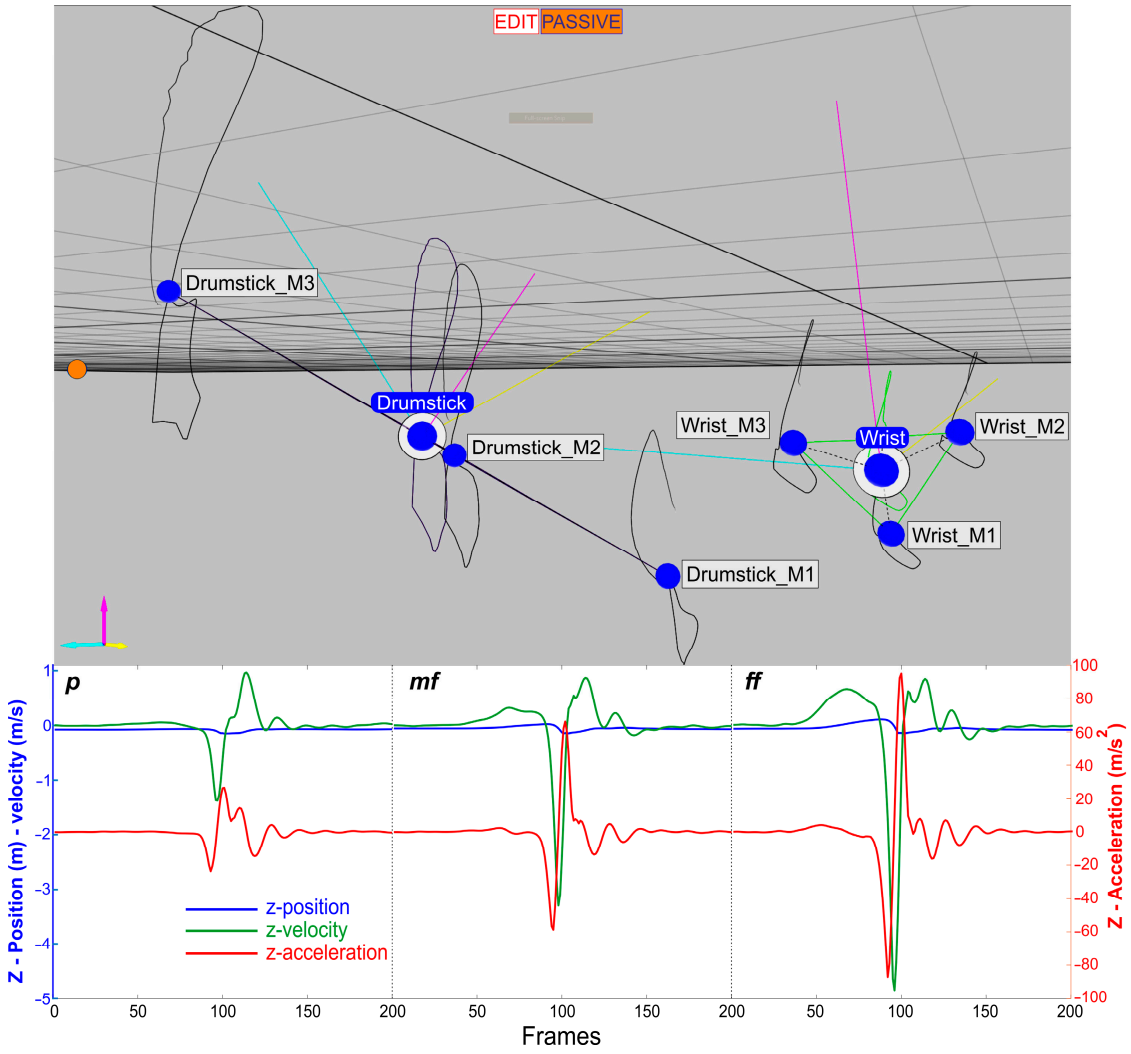

Figure 3. Top: Traces for the *ff* stroke for all three reflective markers and centroids of rigid bodies. Bottom: Vertical position, velocity, and acceleration of drumstick head for the three representative strokes, *p*, *mf*, and *ff*.

5. Results and Discussion

Figure 4 shows representative results of pressure (a,b) and vertical displacement (c,d) for two temporal instants immediately after the drumstick hits the cymbal for the *mf* selected free stroke. The maximum developed stresses on the cymbal at the impact point reach a value of 40 MPa, which is below an estimated tensile yield strength value of 125 MPa [32]; thus, no plastic effects occur. The maximum vertical displacements at the impact point reach a value of 38 μm, while the mean value of the maximum vertical displacements, during the simulation time of 2 s, is approximately 15 μm. What is evident from both depicted quantities in Figure 4 is the generation of bending waves that propagate outwardly from the impact point. These waves are later reflected at the edges of the instrument and lead to standing wave patterns that form the normal vibrational modes [33]. A similar behaviour of the structural characteristics of the cymbal is observed for the models that simulate the *p* and *ff* free strokes. Moreover, the model is capable of providing an estimation time for the contact time; it is computed to be 0.25 ms for the fast *ff* stroke and 0.35 ms for the slower *p* stroke.

Figure 5 shows the sound pressure wave and the sound pressure level (SPL) of the modelled emitted sound for the three progressively intensified free strokes, *p*, *mf*, and *ff*, for the point in the medium of air with coordinates (X,Y,Z) = (0.5,0,0.5) m. An expected

progressive increase of maximum sound pressure level and a progressive decrease of attack time in the amplitude envelopes is apparent from the *p–mf–ff* waveforms presented in Figure 5a. This confirms that the synergy of motion capturing and FEM provides a valid approximation of the dynamic vibroacoustic behaviour of the cymbal owing to the impact of the drumstick. It is also important to report on the maximum computed values of pressure and SPL, which, for the *ff* stroke, are 0.2 Pa and 70 dB, respectively.

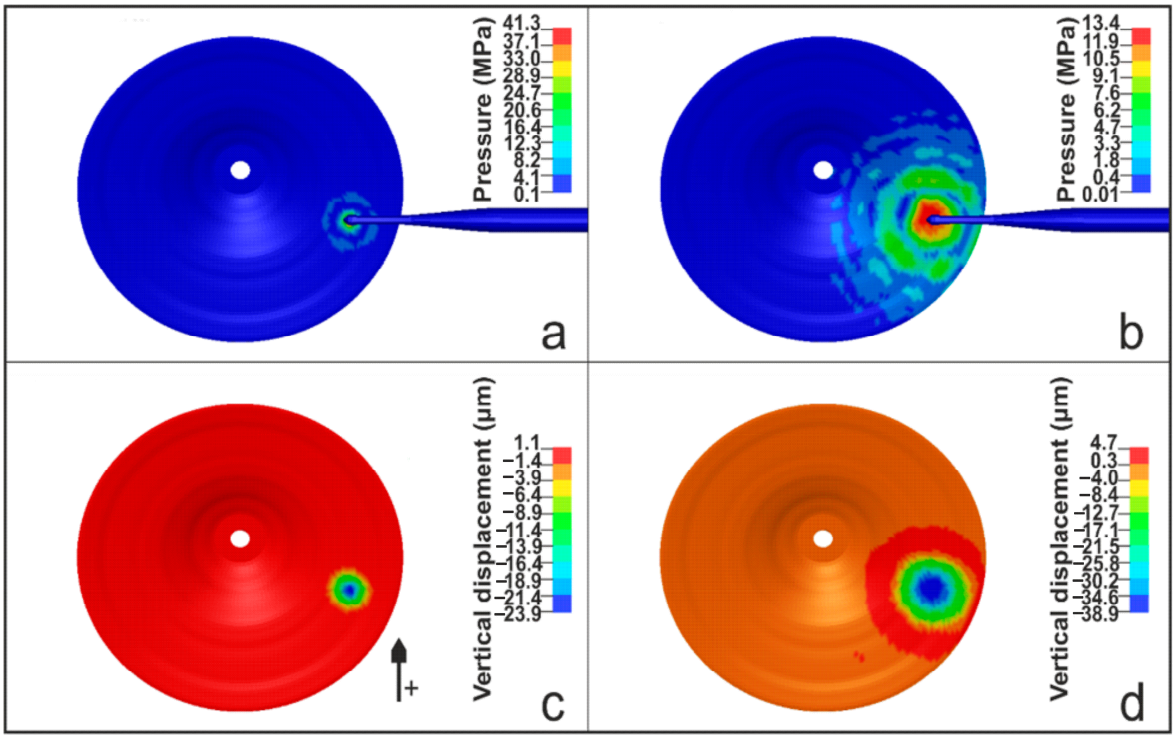

Figure 4. Pressure distribution of the cymbal at (**a**) 0.1 ms and (**b**) 0.3 ms after the drumstick hits the instrument for the *mf* stoke. Vertical displacement of the cymbal at (**c**) 0.1 ms and (**d**) 0.3 ms after the drumstick hits the instrument for the *mf* stroke. The arrow denotes the positive direction of displacements.

Figure 6 shows the time domain FEM-BEM results at the same point (X,Y,Z) = (0.5,0,0.5) m, as represented by the pressure spectrogram of the splash cymbal hit by the *mf* free stroke (Figure 6a) and the velocity spectrogram for the splash cymbal hit by the same stroke (Figure 6b). The results of the pressure and velocity spectrograms have common peak values and trends in temporal behaviour; however, the harmonics developed on the vibrating structure are more clear and more discrete than the harmonics developed in the air. The first spectrogram (sound pressure) exhibits a distinguishable peak structure throughout the entire duration of the observation window. However, it is broad in frequency range. The second spectrogram (velocity) has a wider distribution of energy at the beginning. It appears to fade-out rapidly while maintaining a dense peak structure at the region of lower frequencies at the same time, i.e., below 2 kHz. Both spectrograms adhere well to the noisier signals of percussive sounds in comparison to the high energy concentration of harmonic frequencies that are clearly visible in spectrograms of pitched sounds. However, the velocity spectrogram better highlights the much faster decay of frequencies in the higher region of the spectrum than for those in the lower region. This frequency dependent damping behaviour has been attributed to viscoelastic material properties in the literature [34].

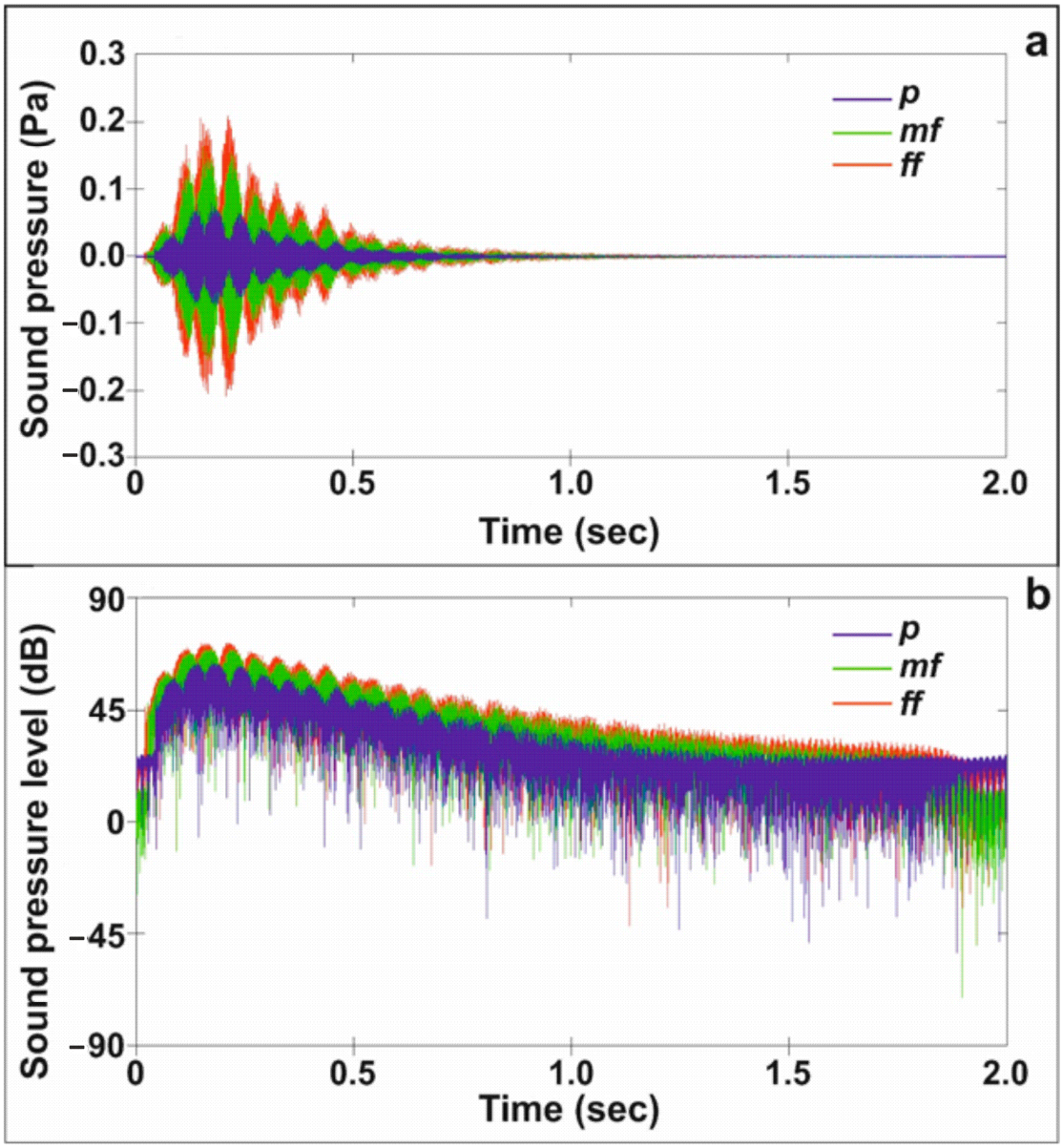

Figure 5. Computed (**a**) sound pressure and (**b**) SPL values of the emitted sound for the three progressively intensified free strokes *p*, *mf*, *ff*.

Figure 7 demonstrates the time domain FEM-BEM results for the same point (X,Y,Z) = (0.5,0,0.5) m, as represented by the pressure spectrogram for the splash cymbal hit by the *p* and *ff* strokes, in Figure 7a and Figure 7b, respectively. It also shows the recorded sound results for the same *p* and *ff* strokes, in Figure 7c and Figure 7d, respectively. Pair-wise visual comparison of *p* vs. *ff* stroke spectrograms indicates a similar relative behaviour in the effect that the stroke intensity has on the produced spectrum for both simulated and recorded sound.

The results presented by this heuristic comparison of the recorded sound with the simulated sound for drum strokes for different performance dynamics indicate the parameters to be improved in the future: namely, the sampling rate of the captured motion data, the material properties, the detailed in sub-mm scale geometrical characteristics of the CAD models, and the sampling rate of the vibroacoustic FEM-BEM simulations. Optimising these key parameters may allow for a direct comparison of the real to the simulated sounds. This is, however, not the focus at the current state of our work.

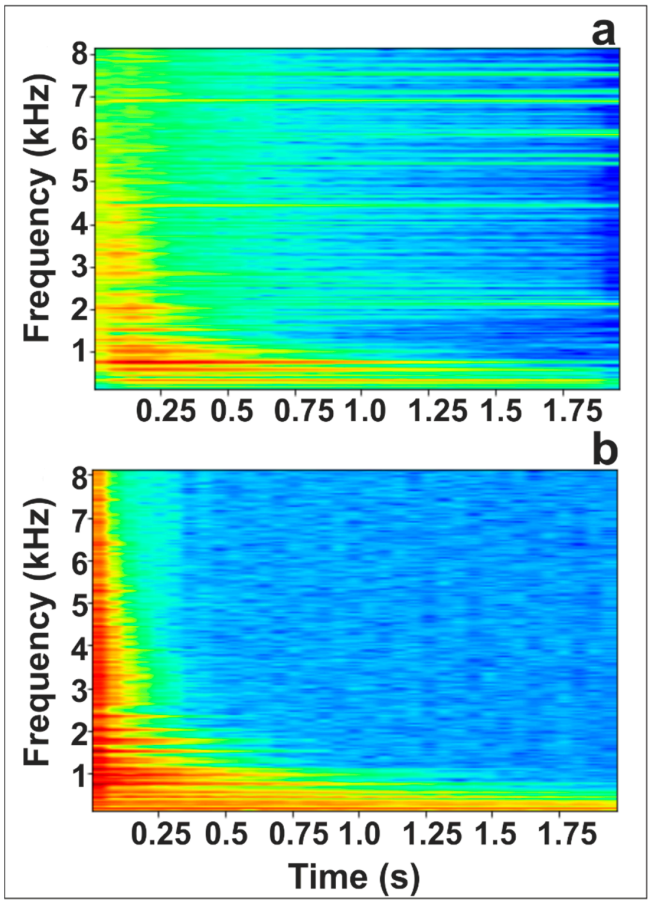

Figure 6. (**a**) Sound pressure spectrograms for the splash cymbal hit by a *mf* free stroke; (**b**) Velocity spectrogram for the splash cymbal hit by a *mf* free stroke.

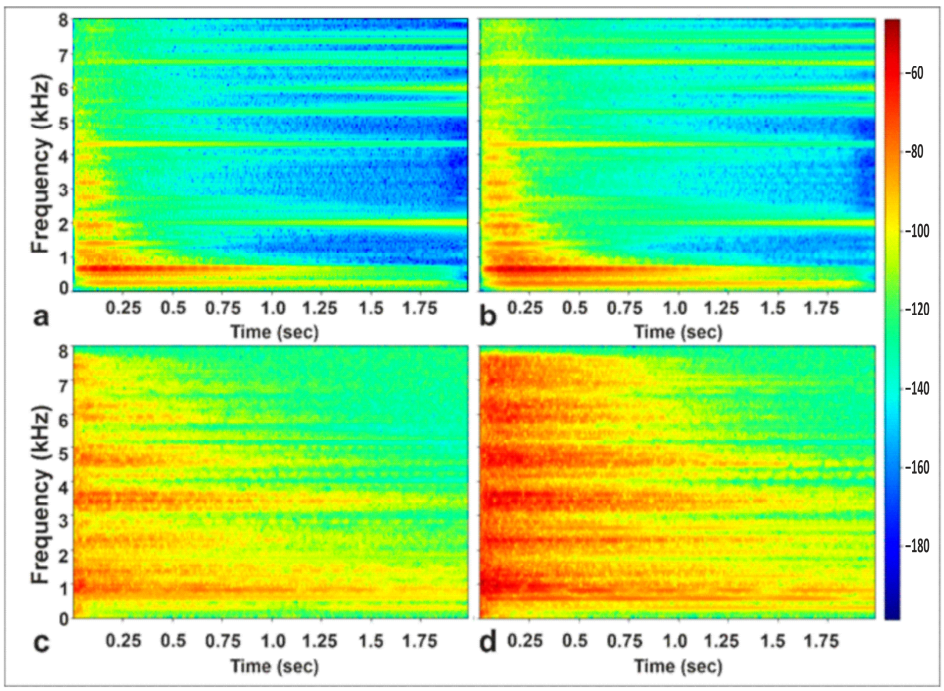

Figure 7. Time domain FEM-BEM results of pressure spectrograms for the splash cymbal hit by (**a**) a *p* free stroke and (**b**) a *ff* free stroke and recorded sound results of the cymbal, for the same (**c**) *p* free stroke and (**d**) *ff* free stroke.

6. Conclusions

This paper proposes a new methodological perspective in vibroacoustic analysis simulations that incorporates the description of the real 3D motion that activates the vibration. The real 3D motion data are recorded from the interaction of a drummer–drumstick–cymbal system and adopted by the FEM-BEM time domain simulations of a musical splash cymbal for progressively intensified free strokes. The model provides insight to the mechanical and acoustodynamic behaviour of the instrument and the contact time of the interaction between drumstick and cymbal. The synergy of motion capturing and the FEM models provide an innovative approximation of the dynamic vibroacoustic behaviour of the cymbal caused by the impact of the drumstick. The progressive increase of maximum sound pressure level and the respective decrease of attack time in the amplitude envelopes can be visually deduced from the presented waveforms of *p–mf–ff* performance dynamics. A heuristic comparison of the simulated to the real sounds with the progressive intensification of real drumstick strokes is presented and demonstrates that increased intensification for both simulated and recorded sound exhibit similar behaviour.

The present study revealed that key parameters affecting the experimental validity of the proposed methodology are the sampling rate of the captured motion data, the material properties, the geometrical details of the CAD models, and the sampling rate of the vibroacoustic simulations. Future developments of FEM-BEM models and the optimization of these parameters will allow for a systematic evaluation of the simulated model through an accurate comparison with the recorded sounds. Furthermore, we plan to assemble an audio dataset that will associate the computed sound signals to the sounds recorded by struck cymbals, under the different drumming conditions identified by the captured motion data. The experimental setup presented in this paper allows performing a large number of sound recordings for different motion-measurable setups.

Author Contributions: Conceptualization, V.D. and E.K.; methodology, E.K. and S.P.; software, E.K. and S.P.; validation, E.K. and S.P.; formal analysis, E.K. and S.P.; investigation, E.K., S.P., C.A. and V.D.; data curation, E.K. and S.P.; writing—original draft preparation, E.K. and S.P.; writing—review and editing, S.P., C.A. and V.D.; supervision, V.D.; All authors have read and agreed to the published version of the manuscript.

Funding: This research received no external funding.

Data Availability Statement: The data presented in this study are available within the article.

Acknowledgments: This work was supported by computational time granted by the Greek Research & Technology Network (GRNET) in the National HPC facility ARIS-under project ID pr011027-LaMPIOS. We would like to thank our undergraduate student and drummer Maxi Kabutz for his assistance in the experimental measurements.

Conflicts of Interest: The authors declare no conflict of interest.

References

1. Pinksterboer, H. *The Cymbal Book*; Mattingly, R., Ed.; Hal Leonard Corporation: Milwaukee, WI, USA, 1992.
2. Rossing, T.D.; Yoo, J.; Morrison, A. Acoustics of percussion instruments: An update. *Acoust. Sci. Technol.* **2004**, *25*, 406–412. [CrossRef]
3. Available online: https://www.moderndrummer.com/2011/10/what-you-need-to-know-about-cymbal-alloys/ (accessed on 8 January 2023).
4. Rossing, T.D.; Peterson, R.W. Vibrations of plates, gongs, and cymbals. *Percuss. Notes* **1982**, *19*, 31–41.
5. Wilbur, C.; Rossing, T.D. Subharmonic generation in cymbals at large amplitude. *J. Acoust. Soc. Am.* **1997**, *101*, 3144. [CrossRef]
6. Perrin, R.; Swallowe, G.M.; Moore, T.R.; Zietlow, S.A. Normal modes of an 18 inch crash cymbal. *Proc. Inst. Acoust.* **2006**, *28*, 653–662.
7. Perrin, R.; Swallowe, G.M.; Zietlow, S.A.; Moore, T.R. The normal modes of cymbals. *Proc. Inst. Acoust.* **2008**, *30*, 460–467.
8. Osamura, K.; Kuratani, F.; Koide, T.; Ogawa, W.; Taniguchi, H.; Monju, Y.; Mizuta, T.; Shobu, T. The Correlation Between the Percussive Sound and the Residual Stress/Strain Distributions in a Cymbal. *J. Mater. Eng. Perform.* **2016**, *25*, 5323–5329. [CrossRef]
9. Kuratani, F.; Yoshida, T.; Koide, T.; Mizuta, T.; Osamura, K. Understanding the effect of hammering process on the vibration characteristics of cymbals. *J. Phys. Conf. Ser.* **2016**, *744*, 12110. [CrossRef]

10. Ducceschi, M.; Touzé, C. Modal approach for nonlinear vibrations of damped impacted plates: Application to sound synthesis of gongs and cymbals. *J. Sound Vib.* **2015**, *344*, 313–331. [CrossRef]
11. Nguyen, Q.B.; Touzé, C. Nonlinear vibrations of thin plates with variable thickness: Application to sound synthesis of cymbals. *J. Acoust. Soc. Am.* **2019**, *145*, 977–988. [CrossRef] [PubMed]
12. Samejima, T. Nonlinear physical modeling sound synthesis of cymbals involving dynamics of washers and sticks/mallets. *Acoust. Sci. Technol.* **2021**, *42*, 314–325. [CrossRef]
13. Tatsuhito, A.; Koki, I. Relationship between chaotic vibrations and acoustic properties of percussion cymbals. *Res. Eng.* **2022**, *14*, 100419.
14. Kaselouris, E.; Alexandraki, C.; Bakarezos, M.; Tatarakis, M.; Papadogiannis, N.A.; Dimitriou, V. A detailed FEM Study on the Vibro-acoustic Behaviour of Crash and Splash Musical Cymbals. *Int. J. Circuits Syst. Signal Process.* **2022**, *16*, 948–955. [CrossRef]
15. Kaselouris, E.; Bakarezos, M.; Tatarakis, M.; Papadogiannis, N.A.; Dimitriou, V. A Review of Finite Element Studies in String Musical Instruments. *Acoustics* **2022**, *4*, 183–202. [CrossRef]
16. Kaselouris, E.; Alexandraki, C.; Orphanos, Y.; Bakarezos, M.; Tatarakis, M.; Papadogiannis, N.A.; Dimitriou, V. Acoustic analysis of impact sound on vibrating circular membranes. In *Proceedings of the INTER-NOISE 2021—2021 International Congress and Exposition of Noise Control Engineering, Washington, DC, USA, 1–4 August 2021*; Institute of Noise Control Engineering: Reston, VA, USA, 2021; Volume 63, pp. 3378–3385.
17. Bakarezos, E.; Orphanos, Y.; Kaselouris, E.; Dimitriou, V.; Tatarakis, M.; Papadogiannis, N.A. Laser-Based Interferometric Techniques for the Study of Musical Instruments. In *Computational Phonogram Archiving*; Springer: Cham, Switzerland, 2019; pp. 251–268.
18. Hallquist, J.O. *LS-DYNA Theory Manual, California*; Livermore Software Technology Corporation: Livermore, CA, USA, 2006.
19. Huang, Y.; Souli, M. Simulation of Acoustic and Vibro-Acoustic Problems in LS-DYNA using Boundary Element Method. In Proceedings of the 10th International LS-DYNA Users Conference, Detroit, MI, USA, 8–10 June 2008.
20. Available online: https://www.thomann.de/gr/zildjian_kregular_8_splash.htm. (accessed on 8 January 2023).
21. Available online: https://www.thomann.de/gr/vic_firth_vfaj6_drumstick.htm. (accessed on 8 January 2023).
22. Meinl. *The Meinl Cymbals Catalogue—Inspire*; Meinl: Gutenstetten, Germany, 2004.
23. Mania, P.; Siuda, F.; Roszyk, E. Effect of Slope Grain on Mechanical Properties of Different Wood Species. *Materials* **2020**, *13*, 1503. [CrossRef] [PubMed]
24. Kaselouris, E.; Dimitriou, V.; Fitilis, I.; Skoulakis, A.; Koundourakis, G.; Clark, E.L.; Chatzakis, J.; Bakarezos, M.; Nikolos, I.K.; Papadogiannis, N.; et al. Preliminary investigation on the use of low current pulsed power Z-pinch plasma devices for the study of early stage plasma instabilities. *Plasma Phys. Control. Fusion* **2017**, *60*, 014031. [CrossRef]
25. Aris Documentation. Available online: http://doc.aris.grnet.gr/system/hardware/ (accessed on 8 January 2023).
26. Paschalidou, S. Effort inference and prediction by acoustic and movement descriptors in interactions with imaginary objects during Dhrupad vocal improvisation. *Wearable Technol.* **2022**, *3*. [CrossRef]
27. Paschalidou, S.; Eerola, T.; Clayton, M. Voice and movement as predictors of gesture types and physical effort in virtual object interactions of classical Indian singing, In Proceedings of the 3rd International Symposium on Movement and Computing (MOCO '16), Thessaloniki, Greece, 5–6 July 2016; Association for Computing Machinery: New York, NY, USA, 2016, 45, 1–2.
28. Dahl, S. Striking movements: A survey of motion analysis of percussionists. *Acoust. Sci. Technol.* **2011**, *32*, 168–173. [CrossRef]
29. Wagner, A. Analysis of Drumbeats: Interaction between Drummer, Drumstick and Instrument. Master's Thesis, Kunglia Tekniska Högskolan, Stockholm, Sweden, 2006.
30. Dahl, S. Movements, timing and precision of drummers. In *Handbook of Human Motion*; Springer: New York, NY, USA, 2018.
31. Schafer, R.W. What is a Savitzky-Golay filter? *IEEE Signal Process. Mag.* **2011**, *28*, 111–117. [CrossRef]
32. Available online: https://www.azom.com/article.aspx?ArticleID=6294. (accessed on 8 January 2023).
33. Schedin, S.; Gren, P.O.; Rossing, T.D. Transient wave response of a cymbal using double-pulsed TV holography. *J. Acoust. Soc. Am.* **1998**, *103*, 1217–1220. [CrossRef]
34. Bader, R. Spectrally-Shaping Viscoelastic Finite-Difference Time Domain Model of a Membrane. *Int. J. Inform. Soc.* **2020**, *12*, 81–93.